THE JOURNAL OF PHYSICAL CHEMISTRY C

Article

Cite This: J. Phys. Chem. C 2019, 123, 29162−29172

pubs.acs.org/JPCC

Unipolar Injection and Bipolar Transport in Electroluminescent Ru-Centered Molecular Electronic Junctions

Ushula M. Tefashe,[†] Colin Van Dyck,[‡] Shailendra K. Saxena,[†] Jean-Christophe Lacroix,[§] and Richard L. McCreery*[,†]

[†]Department of Chemistry, University of Alberta, 11227 Saskatchewan Drive, Edmonton, Alberta T6G 2G2, Canada

[‡]Department of Physics, University of Mons, 20, place du Parc, 7000 Mons, Belgium

[§]University de Paris, ITODYS, CNRS UMR 7086, 15 rue J-A de Baif, F-75013 Paris, France

Supporting Information

ABSTRACT: Bias-induced light emission and light-induced photocurrents were used as independent probes of charge transport in carbon-based molecular junctions containing $Ru(bpy)_3$. The thickness, bias, and temperature dependence of both the total device current and photoemission were compared, as well as their response to bias pulses lasting from a few milliseconds to several seconds. The device current was exponentially dependent on the square root of the applied electric field, with weak dependence on thickness when compared at a constant field. In contrast, light emission was strongly dependent on thickness at a given electric field, with a thickness-independent onset for light emission and a large intensity increase when the bias exceeded the 2.7 V HOMO−LUMO gap of $Ru(bpy)_3$. The apparent activation energies for light emission and current were similar but much smaller than those expected for thermionic emission or redox exchange. Light emission lagged current by several milliseconds but reached maximum emission in 5−10 ms and then decreased slowly for 1 s, in contrast to previously reported solid-state $Ru(bpy)_3$ light-emitting devices that relied on electrochemical charge injection. We conclude that at least two transport mechanisms are present, that is, "unipolar injection" initiated by electron transfer from a $Ru(bpy)_3$ HOMO to the positive electrode and "bipolar injection" involving hole and electron injection followed by migration, recombination, and light emission. The unipolar mechanism is field-driven and the majority of the device is current, while the bipolar mechanism is bias-driven and involves electrode screening by PF_6 ions or mobile charges. In addition, significant changes in thickness and temperature dependence for thicknesses exceeding 15 nm imply a change from injection-limited transport to bulk-limited transport. The current results establish unequivocally that electrons and holes reside in the molecular layer during transport once the transport distance exceeds the ∼5 nm limit for coherent tunneling and that redox events involving nuclear reorganization accompany transport. In addition, they demonstrate luminescence in a single organometallic layer without hole or electron transport layers, thicknesses below 30 nm, and symmetric electrodes with similar work functions.

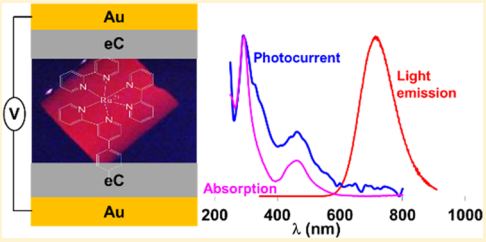

INTRODUCTION

The field of molecular electronics investigates charge transport in mainly organic molecules across distances (d, nm) as short as one molecule (∼1 nm) up to ∼30 nm, motivated in part by the ability to modify transport and electronic properties by changes in molecular structure, sometimes dubbed "rational design". Transport mechanisms over 1−30 nm may involve tunneling and other mechanisms that differ fundamentally from those reported for the >50 nm distances commonly encountered in thin-film transistors[1−5] and organic light-emitting diodes (OLEDs)[6−8] widely studied in the field of organic electronics. Many studies of single molecule and "ensemble" molecular junctions (MJs) have concluded that quantum mechanical tunneling is the dominant mechanism for aliphatic molecules with d < 2 nm or conjugated molecules with d < 5 nm. For d > 5 nm and aromatic molecules, a transition from tunneling to a different, often activated mechanism has been reported and attributed to resonant transport,[9−11] field ionization,[12] Schottky injection,[13] and hopping mediated by activated, Marcus-like polaron transport between subunits in an oligomer.[14,15] Transport in some cases with d > 5 nm is temperature-dependent, with apparent activation energies (E_{act}) of 200−300 meV,[14,15] while other examples exhibit E_{act} < 100 meV over a range of 200−300 K or are activationless, with E_{act} being statistically zero below 200 K.[11,12,16,17] In the case of bis-thienyl benzene oligomers between carbon electrodes, current densities exceeding 10 A/cm^2 were observed across 22 nm and T < 10 K when the applied bias exceeded 5 V.[12]

Molecular junctions with d in the range of 2−40 nm, which contain metal centers (Ru, Co, Fe, etc.), are of interest to charge transport mechanisms due to redox levels, which may

Received: October 26, 2019
Revised: November 5, 2019
Published: November 6, 2019

DOI: 10.1021/acs.jpcc.9b10076
J. Phys. Chem. C 2019, 123, 29162−29172

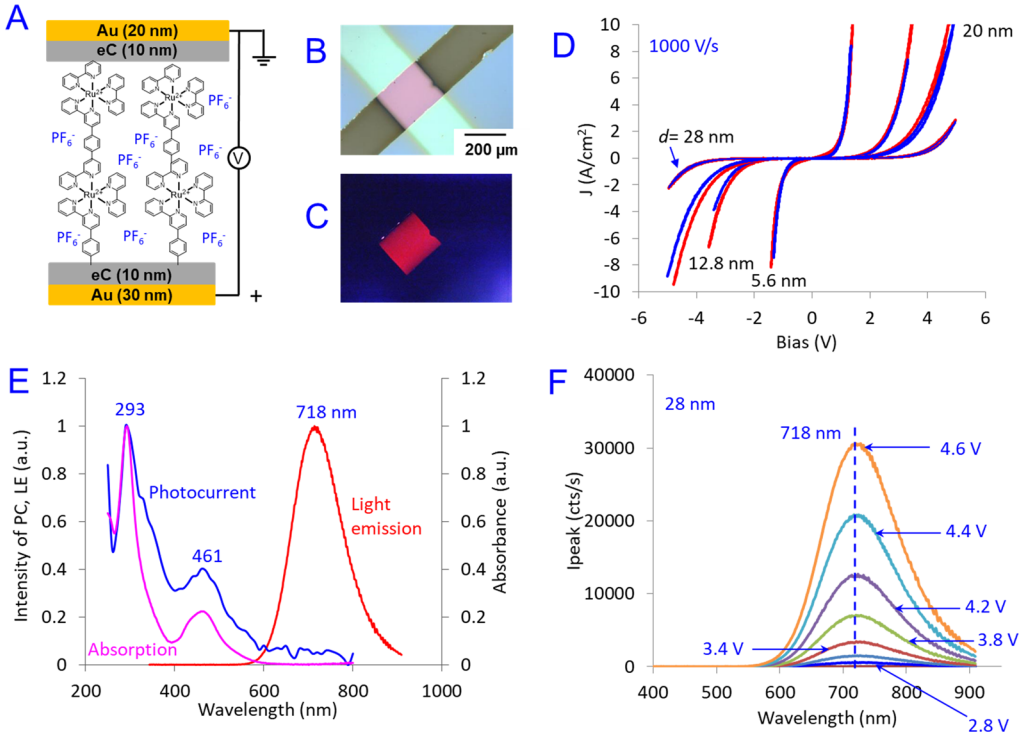

Figure 1. (A) Schematic illustration of the $Cr_4/Au_{30}/eC_{10}/Ru(bpy)_3/eC_{10}/Au_{20}$ molecular junction, with subscripts indicating layer thicknesses in nanometers. Polarity is always stated as the bottom relative to the top contact, and light emission is monitored above the top contact. Optical images of 12.8 nm $Ru(bpy)_3$ molecular junctions with a scale bar: (B) no bias in room light and (C) under 3.4 V bias in darkness. (D) *JV* curves at a scan rate of 1000 V/s of $Cr_4/Au_{30}/eC_{10}/Ru(bpy)_3/eC_{10}/Au_{20}$ in vacuum (red curve) and acetonitrile vapor (blue curve) for d = 5.6, 12.8, 20, and 28 nm. (E) UV−vis absorption, photocurrent, and light emission spectra for 12.8 nm $Ru(bpy)_3$ MJs. (F) Light emission spectra from 28 nm $Ru(bpy)_3$ junctions for a positive bias with V_{app} = 2.8, 3.2, 3.4, 3.8, 4.2, 4.4, and 4.6 V.

be involved in long-range transport.[9,10,13,16,18−20] Of particular relevance is the bipyridyl complex of ruthenium, $Ru(bpy)_3$, since it can emit light and has been studied extensively in solid-state electrochemiluminescence[21−24] and in OLEDs.[25−28] Past examples of light-emitting solid-state $Ru(bpy)_3$ devices had >50 nm-thick molecular layers and involve electrochemical generation of Ru^{+1} at one electrode and Ru^{+3} at the opposing electrode followed by diffusion and recombination to produce excited Ru^{+2}*, which emits light. As discussed below, such devices have a slow onset of light emission (seconds to minutes) and often rely on ion motion to establish ionic double layers, which promote redox reactions at the electrode interfaces.[21,22,25,29]

We reported recently that MJs containing single layers of $Ru(bpy)_3$ oligomers (d = 4 to 13 nm) emit light when d exceeds ∼6 nm and are stable for ∼10 h of continuous light emission (LE) under a bias of 2.8 V.[30] Unlike most OLEDs, the $Ru(bpy)_3$ MJs had symmetric carbon electrodes and had behavior distinct from light-emitting electrochemical cells (LEC) or $Ru(bpy)_3$ OLEDs, including a much faster LE rise time, insensitivity to polarity, and weak dependence on solvent or ion mobility. Using the LEC mechanism as a precedent, we proposed a bipolar injection mechanism, in which both holes and electrons are injected from the corresponding electrodes and excited Ru^{+2}* molecules are formed in the MJ interior, which then emit light. Given the context of previous investigations of light emission by solid-state $Ru(bpy)_3$-containing devices, the current investigation was directed toward four questions: (1) Is ion motion involved or necessary for efficient light emission at a low voltage? (2) Do the shorter transport distances in molecular junctions and resulting high electric fields significantly modify the transport mechanism compared to LECs with d > 50 nm? (3) What does light emission reveal about transport in MJs with thicknesses beyond the limit of coherent tunneling (∼5 nm)? (4) Can light emission provide insights into the transport mechanism, notably unipolar injection versus bipolar injection? The variation of MJ current and LE magnitudes and rise times with an applied bias, $Ru(bpy)_3$ layer thickness, temperature, and solvent vapor provide strong support for two transport mechanisms, one of which results in light emission.

METHODS

Molecular junction fabrication, electrochemical grafting, thickness measurements, and current−voltage characterization used previously published procedures.[16,30,31] Grafting conditions and layer thicknesses determined by atomic force microscopy are provided in Section S7, Supporting Information. Ru(bpy) MJs were biased with a Keithley 2602A source measurement unit, and the light emission spectra were acquired with a spectrograph/charge-coupled device (CCD) using a procedure described previously.[32] Briefly, an optical microscope with a 50× objective was interfaced to a spectrograph (Andor Shamrock SR-303i-B with an Andor Newton CCD detector) with an optical fiber. The MJ devices were measured at room temperature in vacuum of $<10^{-4}$ torr to minimize water interference. The observed spectra were corrected for the wavelength-dependent sensitivity of the detector using a standard calibration process with a blackbody lamp (Ocean Optics LS-1-CAL or HL2000) to obtain the spectral intensity (i.e., the intensity per unit wavelength).[32,33] Current and light emission transients were measured using a custom Labview

DOI: 10.1021/acs.jpcc.9b10076
J. Phys. Chem. C 2019, 123, 29162−29172

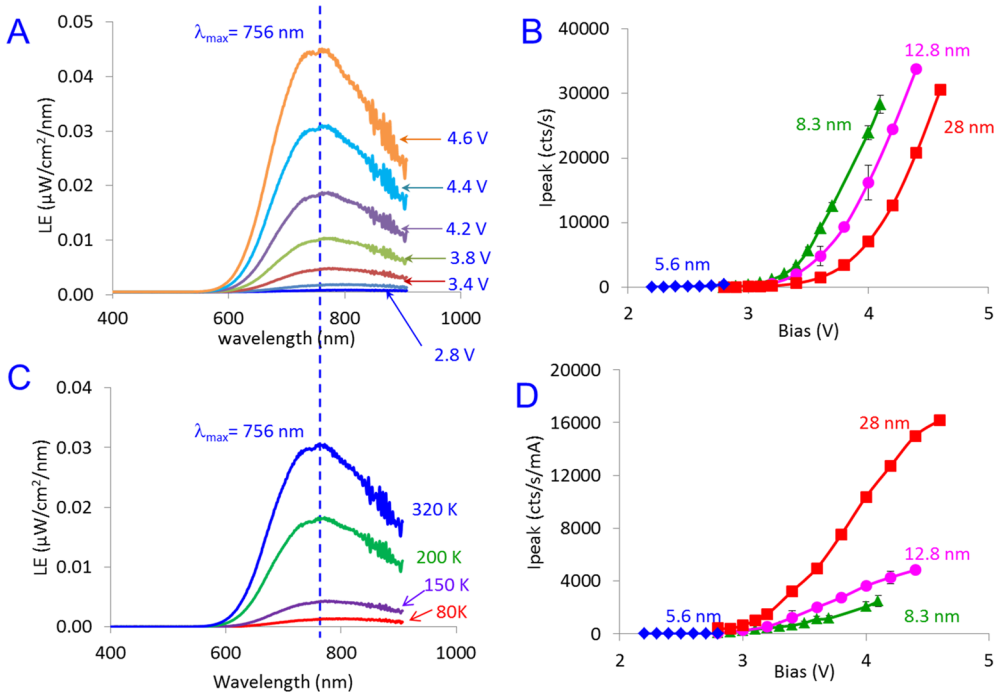

Figure 2. (A) Spectra of Figure 1F after correction for instrument response. (B) Peak emission intensity as a function of junction bias for three different thicknesses (8.3, 12.8, and 28 nm). (C) Corrected light emission spectrum of the 12.8 nm $Ru(bpy)_3$ junction measured at +3.2 V bias and variable temperature (80, 150, 200, and 320 K). (D) Peak emission intensity normalized to junction current versus applied positive bias from $Ru(bpy)_3$ MJs with d = 5.6, 8.3, 12.8, and 28 nm. Error bars provided for 8.3 and 12.8 nm are standard deviations and, in some cases, are smaller than the data points.

system, with light monitored by an Andor Si detector (Andor SR-ASM-0046 UV enhanced silicon detector) and an SRS 570 current amplifier. The spectral response of the Andor Si detector is provided in Figure S5, Supporting Information. LE versus temperature was acquired with a fiber optic-coupled, 40 mm focal length lens (OZ Optics), with the fiber coupled directly to the Si detector, and provided a 50 mm working distance sufficient to monitor LE in a Janis cryogenic probe station. The photocurrent experiment in Figure 1E used previously published procedures.[17] Briefly, a 150 W Xenon arc source was attached with a monochromator through an optical beam chopper and focused onto the MJ through the top contact. Photocurrent detection was done using a lock-in amplifier referenced to the optical beam chopper. *JV* curves in Figure 1 are averages of at least four MJs for each thickness, and transient responses of current and light emission were replicated at least three times. Examples of reproducibility are provided in the Supporting Information.

RESULTS

As shown schematically in Figure 1A, the $Ru(bpy)_3$ molecular junction (MJ) consists of oligomers of phenyl-$Ru(bpy)_3$ subunits formed by electrochemical reduction of a diazonium reagent made in situ from the corresponding aromatic amine.[16,30] X-ray photoelectron and Raman spectroscopies are consistent with retention of the $Ru(bpy)_3$ center and the PF_6^- anions in the molecular layer, and the molecular layer thickness (d) could be varied by the reduction conditions of the diazonium precursor.[30] Figure 1B shows an image of a 250 by 250 μm MJ with a top eC_{10}/Au_{20} electrode, which is ~40% transparent to visible light. Figure 1C is an image of a $Ru(bpy)_3$ MJ (d = 12.8 nm) under an applied bias of 3.4 V, with the only source of light being the MJ itself, indicating approximately uniform light emission over the entire junction area. Light emission has equal intensity for either a positive or negative bias and is stable for more than 8 h of continuous operation when encapsulated in a parylene film.[30] Detailed current/voltage responses for the $Ru(bpy)_3$ MJs with d = 1.5 to 28 nm have been reported previously[16] and exhibited two regions in the attenuation plots (ln J vs d). For d < 5 nm, the current decreased exponentially with increasing d when plotted versus applied bias or electric field. When d ranged from 10 to 28 nm, J was nearly constant with thickness at a given electric field (Figure 2C,D from ref 16). Several additional examples are provided in Figure 1D to demonstrate the effect of acetonitrile (ACN) vapor on $Ru(bpy)_3$ MJs. ACN vapor caused a major decrease in the current density versus bias (*JV*) response for MJs containing lithium benzoate, attributed to mobilization of Li^+ and partial screening of the applied electric field.[34] However, in LEC-based devices, removing the residual solvent drastically reduced the current, and LE required a much higher bias voltage to be observed.[27] The small effect of ACN on the *JV* response for $Ru(bpy)_3$ MJs is a first indication that possible motion of the PF_6^- ions is a minor effect for the 1000 V/s scan rates used for Figure 1D and the 5.6 to 28 nm thickness range.

Light emission (LE) was visible to the unaided eye and was monitored quantitatively with a spectrograph/CCD interfaced to a microscope for complete spectra[32,33] or with a single silicon photodetector placed directly above the MJ to record transients. An uncorrected CCD output (A/D counts/s) versus wavelength spectrum for a 12.8 nm $Ru(bpy)_3$ MJ is shown in Figure 1E, along with the absorption spectrum of the active layer in a complete MJ and the photocurrent spectrum at zero bias. As described in detail for other molecules, the photocurrent tracks the optical absorption spectrum, and its

DOI: 10.1021/acs.jpcc.9b10076
J. Phys. Chem. C 2019, 123, 29162−29172

Table 1. Examples of Solid-State $Ru(bpy)_3$ Light-Emitting Devices

system	$Ru(bpy)_3$ thickness (nm)	peak wavelength	rise time (300 K)	reference
ITO/$Ru(bpy)_3$/Al	70−180		15 min @ 3 V, 5 s @ 4.5 V	25
ITO/$Ru(bpy)_3$/Au	100			22
ITO/$Ru(bpy)_3$/In:Ga	100	660 nm	2 s @ 3 V	26
ITO/$Ru(bpy)_3$/In:Ga or Ga:Sn	100		50 s @ 2.75 V (drybox), 2−5 s (air)	21
Au/eC/$Ru(bpy)_3$/eC/Au	12.8	718 nm (756 nm)[a]	4−7 ms @ 3 V	this work

[a]After instrumental response correction.

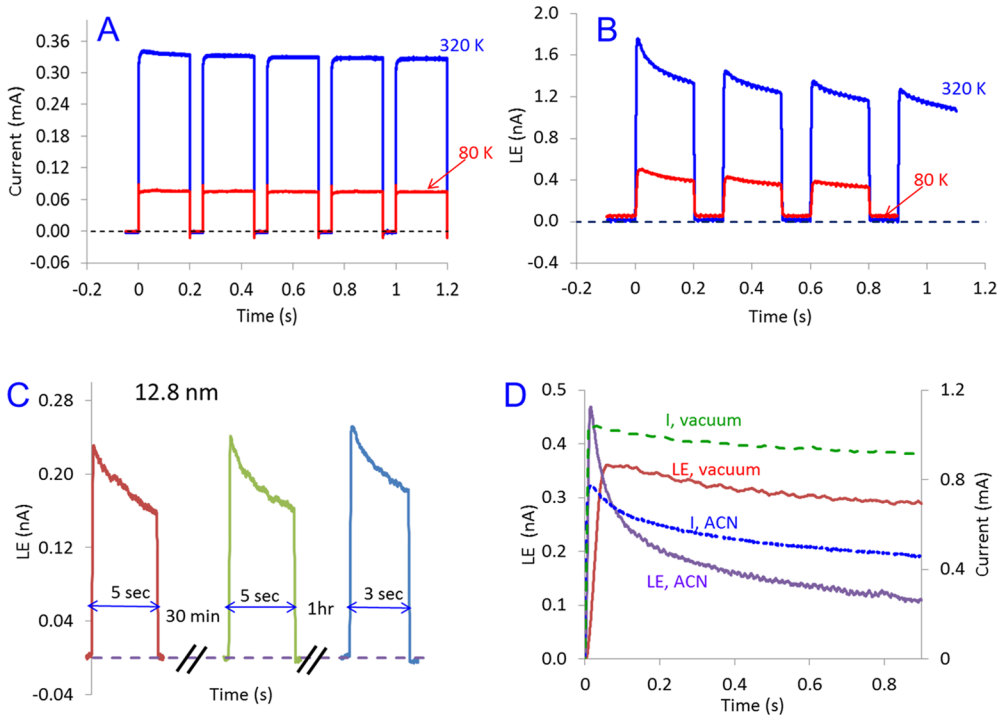

Figure 3. (A) Repeated current versus time at 3.0 V and (B) light emission versus time for a bias pulse of 3.2 V at 80 and 320 K under vacuum (d = 12.8 nm). (C) Total light emission versus time under acetonitrile vapor for bias pulses of 3.2 V and repeated pulses for MJ at rest for several minutes after a bias pulse. (D) Current versus time (dashed lines) and total light emission versus time (solid lines) for bias pulses of 3.2 V at room temperature under vacuum and acetonitrile vapor.

sign correlates with whether the highest occupied molecular orbital (HOMO) or lowest unoccupied molecular orbital (LUMO) is closer in energy to the electrode Fermi level.[17] For $Ru(bpy)_3$ MJs, the positive photocurrent indicates that the HOMO is closer to the electrode Fermi level than the LUMO and implies that transport involves holes as the main carriers. Figure 1F shows the bias dependence of photoemission for d = 28 nm, with a minimal change in the spectrum shape and peak wavelength with a bias. Uncorrected spectra were reported previously for LE by thicker films of $Ru(bpy)_3$ polymers and was attributed to electrochemical charge injection at both electrodes followed by migration of Ru^{+1} and Ru^{+3} by redox exchange followed by generation of excited Ru^{+2}* and LE.[23,25,27] An example is shown in Figure S1 (Supporting Information) for an ITO/$Ru(bpy)_3(ClO_4)_2$/Ga:In device monitored with a CCD. The uncorrected maximum emission wavelength of 660 nm was longer than the ∼610 nm wavelength observed in solution, and the rise time to maximum LE was 1−2 s at room temperature. Uncorrected spectra for the current devices have emission maxima of 718 nm for T = 320 K, and the spectra change little with decreasing temperature to 80 K. Correction of the spectra of Figure 1F for CCD response by comparison to a white light source[32] yields the spectra of Figure 2A with six bias values and is red-shifted approximately 100 nm compared to that of ECL in solution and ∼50 nm compared to the $Ru(bpy)_3$ polymer in an ITO/Ga:In LEC. The red shift in the current devices provides an initial indication that their LE mechanism differs from previous LEC devices based on $Ru(bpy)_3$. Additional uncorrected spectra of light emission for 5.6, 12.8, and 28 nm $Ru(bpy)_3$ junctions are provided in Figure S2, Supporting Information. Figure 2B shows the peak intensity for four different MJs with d = 5.6 to 28 nm, and Figure 2D shows the same data replotted as peak intensity per milliampere of junction current. Both show onsets above ∼2.7 V, and the emission efficiency increases significantly with thickness. As apparent from Figure 2C, photoemission decreases with lower temperature but with minor changes in shape. Additional results regarding temperature are presented below.

LEC experiments often involve ion motion and double layer formation, with a significant rise time of LE following initiation of an applied bias, as described in several reports summarized in Table 1. Delay times of several minutes in solid-state $Ru(bpy)_3$ LE devices were attributed to counterion motion but could be decreased to a few seconds by an initially large bias pulse.[25] As an example, the LEC of Bard and Gao (spectrum

DOI: 10.1021/acs.jpcc.9b10076
J. Phys. Chem. C 2019, 123, 29162−29172

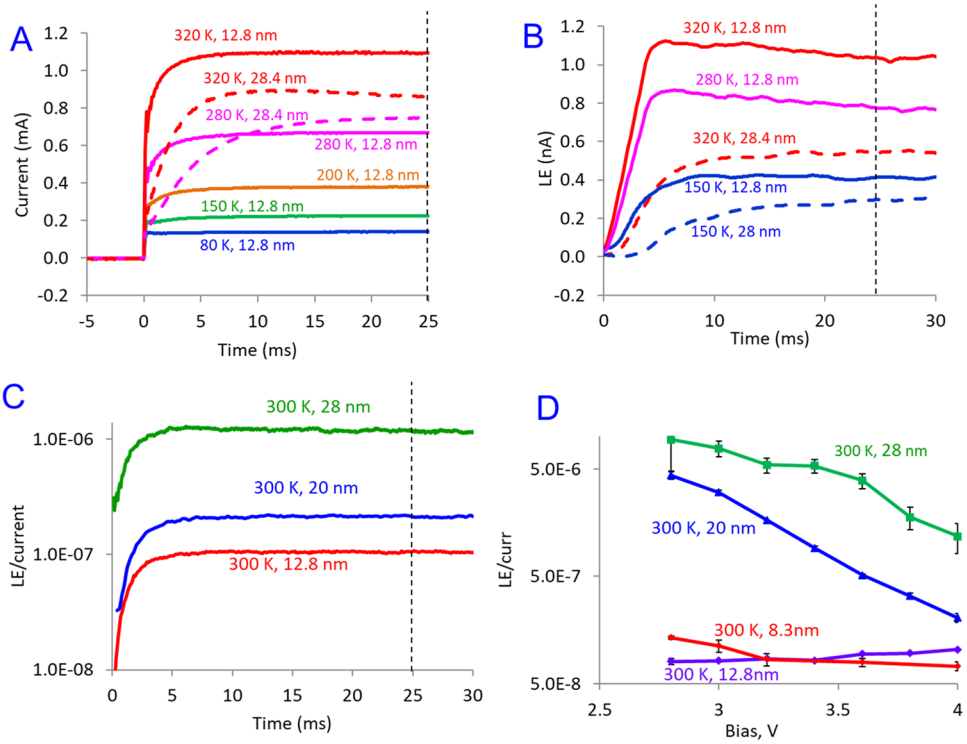

Figure 4. (A) Current transients and (B) light emission transients for bias steps from $V = 0$ to 3.0 V for 12.8 nm $Ru(bpy)_3$ MJs and $V = 0$ to 3.2 V for 28 nm $Ru(bpy)_3$ MJs in vacuum at four temperatures. (C) Light emission-to-current ratio versus time for 12.8, 20, and 28 nm $Ru(bpy)_3$ MJs in vacuum at 300 K. (D) Light emission-to-current ratio versus bias in vacuum at 300 K for $Ru(bpy)_3$ MJs of different thicknesses (8.3, 12.8, 20, and 28 nm), all evaluated at $t = 25$ ms. Error bars indicate standard deviations and, in many cases, are smaller than the data points.

shown in Figure S1) had rise times of 1−5 s to reach maximum emission, although light emission began as little as 20 ms after the bias was applied.[26] Both the rise time and emission intensity depended strongly on polarity, the presence of water or solvent vapor, and the counterion identity, leading to the proposal that LE depended on establishing an electrochemical double layer, which permitted redox reactions.[23,26,27] Figure 3A shows current versus time transients of a eC/$Ru(bpy)_3$/eC MJ with $d = 12.8$ nm for five successive 200 ms bias pulses to +3 V. The rise time of junction current is <50 μs, following a charging current with an observed RC time constant of ∼5 μs (shown in Figure S3, Supporting Information). The current for $T = 320$ K is constant for subsequent pulses after a small decrease (<5%) during the first pulse. At $T = 80$ K, the current was smaller and did not show an observable decrease with time or repetition. LE in response to 200 ms bias pulses shown in Figure 3B decreases by ∼25% during the initial 200 ms at either 320 or 80 K, and the decrease continues during subsequent pulses. Figure 3C shows 5 s pulses to +3 V with a wait period of 30 or 60 min between pulses at 300 K, during which the MJ was at zero bias. The LE recovered or exceeded its initial intensity during the wait periods, indicating that the intensity decrease is not due to irreversible changes in device performance. Figure 3D shows LE from a single junction in vacuum at 300 K before and after exposure to acetonitrile (ACN) vapor for 30 min. ACN enters the junction and mobilizes ions, which both magnifies and accelerates the decrease in LE with time, with a much shorter rise time but a 76% decrease during a 1 s pulse to +3 V at $T = 300$ K. As was the case in vacuum, the LE recovered after a wait period of ∼30 min, and the LE decay was reproducible for at least three pulses in ACN vapor. The results of Figure 3 for slow bias pulses permit several observations. First, the MJ current is constant and repeatable at both 320 and 80 K, although the LE exhibits a decay over a period of ∼100 ms, which is recovered and repeatable after resting at zero bias. Second, both current and LE are activated but are still present at $T = 80$ K, with more details regarding temperature dependence below. LE is observable to the eye even for $T < 10$ K. Third, the LE rise time is shorter, and the decay of LE following bias initiation is more rapid in ACN vapor but also recovers more quickly during resting and $V = 0$. The behavior of the MJs is in stark contrast to that of previous $Ru(bpy)_3$ devices listed in Table 1, with a negative response of both current and LE when possible ion motion is allowed to occur with time, solvent vapor, or higher temperature. Both current and LE are considered next for much shorter time scales.

The solid curves in Figure 4A show selected current versus time responses for a 12.8 nm $Ru(bpy)_3$ MJ for a +3.0 V bias pulse at temperatures from 80 to 320 K in vacuum, with additional temperatures and thicknesses provided in Figure S4. The observed rise time of ∼100 μs is weakly dependent on temperature, while the intensity plateau reached within 10 ms decreases with temperature, as discussed later. The dashed curves are from a 28 nm-thick MJ at 320 and 280 K and an applied bias of 3.2 V and show a slower rise time, which increases significantly with decreasing temperature. LE from the same MJs was monitored in vacuum with a silicon photodetector, with the results shown in Figure 4B. The LE response for both thicknesses has a different shape from the current transients, with slower rise times and a discernible lag in LE response for $d = 28$ nm. Figure 4C shows the ratio of LE to current versus time for three thicknesses and $T = 300$ K on a logarithmic scale. Although both current and LE have slower

DOI: 10.1021/acs.jpcc.9b10076
J. Phys. Chem. C 2019, 123, 29162−29172

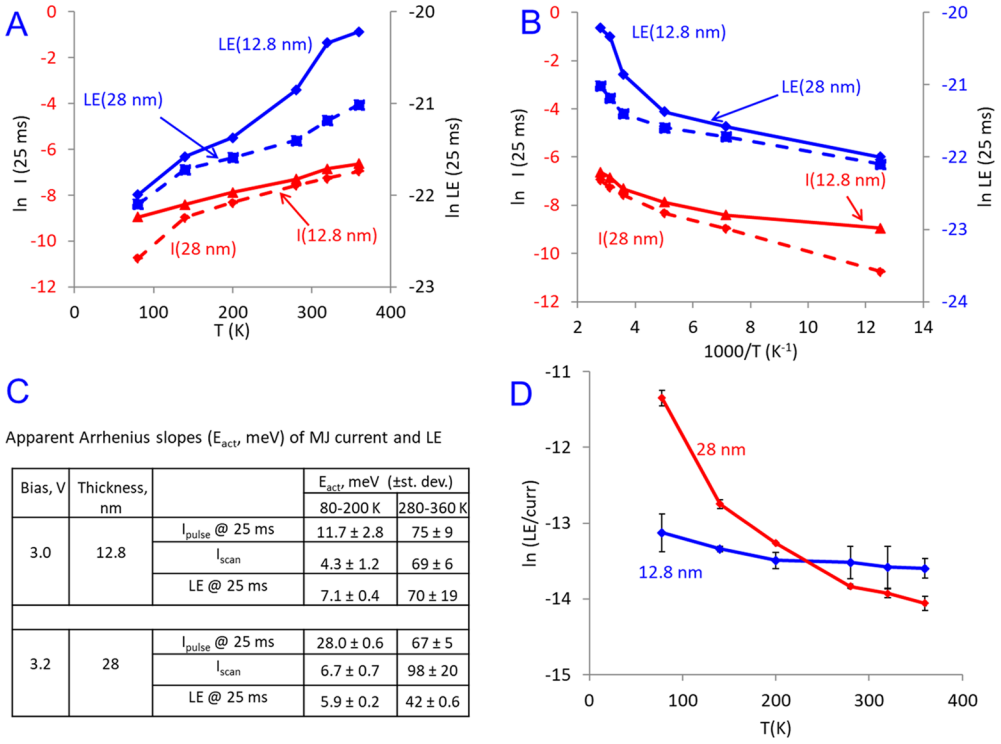

Bias, V	Thickness, nm		E_{act}, meV (±st. dev.)	
			80-200 K	280-360 K
3.0	12.8	I_{pulse} @ 25 ms	11.7 ± 2.8	75 ± 9
		I_{scan}	4.3 ± 1.2	69 ± 6
		LE @ 25 ms	7.1 ± 0.4	70 ± 19
3.2	28	I_{pulse} @ 25 ms	28.0 ± 0.6	67 ± 5
		I_{scan}	6.7 ± 0.7	98 ± 20
		LE @ 25 ms	5.9 ± 0.2	42 ± 0.6

Figure 5. (A) Plots of ln(I) and ln(LE) versus temperature at 3.0 V for 12.8 nm and 3.2 V for 28 nm $Ru(bpy)_3$ junctions. (B) Arrhenius plots of (A) in vacuum. (C) Table of apparent Arrhenius slopes of MJ current and LE. (D) Light emission-to-current ratio versus temperature for 12.8 nm (at 3.0 V) and 28 nm (at 3.2 V) $Ru(bpy)_3$ MJs in vacuum. Error bars are ±standard deviation.

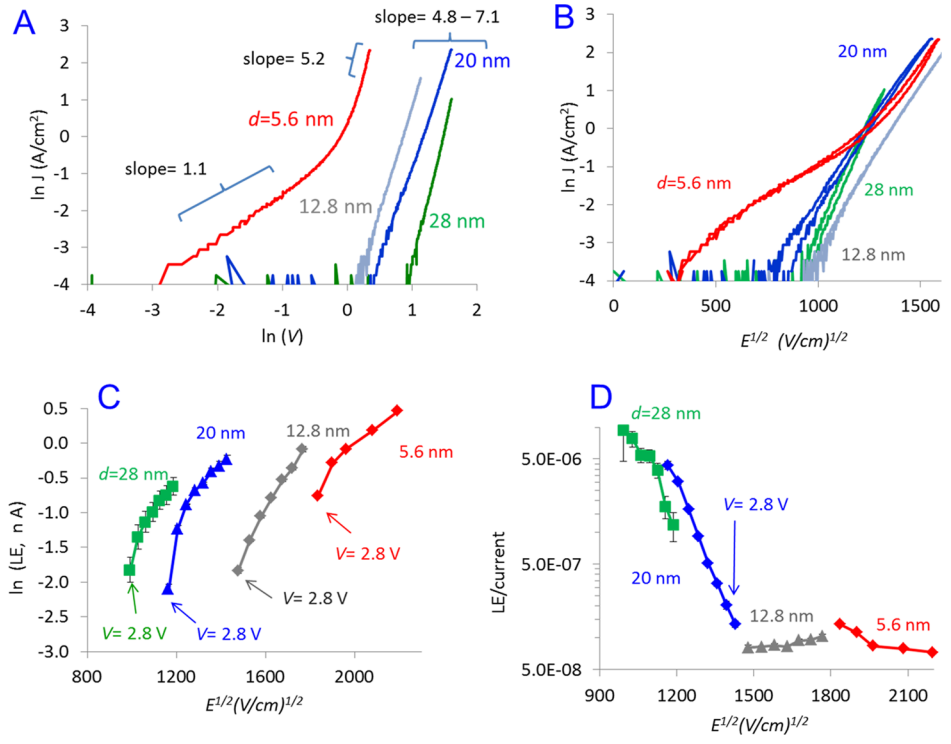

Figure 6. (A) ln J versus ln V plots for different thicknesses of $Ru(bpy)_3$. (B) ln J versus $E^{1/2}$ plots of (A). (C) ln(LE) versus $E^{1/2}$ plots for different thicknesses of $Ru(bpy)_3$ junctions. (D) Light emission to current ratios versus $E^{1/2}$ plots for different thicknesses of $Ru(bpy)_3$. Error bars for higher E plots are within the size of the data points.

rise times for d = 28 nm, the transient response of the LE/current ratio is thickness-independent, implying constant emission efficiency after ~5 ms. The bias and thickness dependence of the LE/current ratio at 300 K were examined for four $Ru(bpy)_3$ thicknesses for a pulse time where both LE and current had reached plateaus (25 ms for 12.8, 20, and 28 nm; 10 ms for 8.3 nm). As shown in Figure 4D, the LE/current ratio is approximately constant for V = 2.8 to 4 V for the two

DOI: 10.1021/acs.jpcc.9b10076
J. Phys. Chem. C 2019, 123, 29162−29172

thinner MJs. For d = 20 and 28, the ratio is much higher overall and decreases with increasing bias, indicating that the efficiency of LE is higher for the thicker MJs operated at low bias. An important observation from Figure 4 is that the distinct pulse responses for the current and LE imply that they are governed by different mechanisms and that this difference is most pronounced for thick MJs compared to thin MJs.

The temperature dependence of both current and light emission from the transients shown in Figure 4 is shown on a logarithmic scale versus temperature in Figure 5A and in Arrhenius format in Figure 5B. All readings in Figure 5 were obtained at t = 25 ms after initiation of a bias pulse, which is the approximate plateau of both current and LE transients (indicated by vertical dashed lines in Figure 4A−C). Note that the scales are different for LE and current; hence, the graphs are useful for comparing trends rather than relative magnitudes. The Arrhenius plots are nonlinear over the 80 to 360 K range, but their low and high T slopes are provided in Figure 5C to permit comparison to activation energies reported for transport in related devices. The apparent Arrhenius slopes of the current at 25 ms are similar to those derived from current−voltage behavior previously,[16] with values of 6−28 meV below 200 K and 40−80 meV in the 280−360 K range. Since both LE and current were determined at t = 25 ms, their ratio provides an indication of LE efficiency, which is plotted versus T in Figure 5D. Note that this ratio decreases slightly with T for d = 12.8 nm, but for d = 28 nm, it increases significantly at a low temperature by a factor of 15 for 80 K compared to 360 K. The magnitude of the LE efficiency depends on thickness, bias, and T, but the large changes apparent in Figure 5D imply that the transport and light emission mechanisms have quite different temperature dependencies.

Previous reports from our laboratory[12,16,35] and also that of Karipidou et al.[13] noted that the current in relatively thick (d > 4 nm) MJs, including those containing metal centers, exhibited linearity of ln J with the square root of the applied bias, that is, $V^{1/2}$. This relation was investigated further with the current $Ru(bpy)_3$ MJs, with the results shown in Figure 6 for both current and light emission. Figure 6A compares plots of ln J versus ln V from the data in Figure 1D, with the low-bias region for d = 5.6 nm having a slope close to unity, which is expected for ohmic behavior. A transition from a slope of 1.0 to 2.0 is often observed in organic semiconductors at high bias, attributed to a transition from ohmic to space charge-limited conduction (SCLC).[36] For the current MJs, a transition occurs for d = 5.6 nm but to a slope of 5.2, with the thicker MJs all exhibiting slopes of 5−7 in the ln J versus ln V format. Furthermore, plotting the same results as ln J versus the square root of the electric field ($E^{1/2}$) shows that all thicknesses approximately overlap when E exceeds ∼1.5 MV/cm. This behavior at high E is consistent with a field-driven transport mechanism rather than a bias-driven transport mechanism, as noted previously,[16] and will be discussed further below. Figure 6C shows the light emission response (LE) versus $E^{1/2}$, with the LE detector current obtained 25 ms after initiation of a bias pulse (the same data as that shown in Figure 4). LE and current plots are obviously very different, with ln(LE) being nonlinear despite a limited range of E and no overlap of LE for varying thicknesses. Although the onset of LE occurs at quite different $E^{1/2}$ values for the four thicknesses, the onset in all cases is at or just below V = 2.8 V. Since current and LE were both determined at t = 25 ms, it is possible to plot the efficiency (LE/current) versus $E^{1/2}$ in Figure 6D, with the y-axis in a logarithmic scale. Although weak LE is observed for d < 15 nm, efficiency increases greatly once a bias of 2.7 V is exceeded. The external quantum efficiency as emitted photon per electron of the MJ current was determined using a standard light source and integration over all emitted wavelengths, as described previously,[30,33] and exceeded 1% for d = 28 nm and V = 3.2 V.

DISCUSSION

The ability to monitor light emission permits direct comparison of the dependence of both device current and LE as functions of bias, temperature, molecular layer thickness, and solvation. Several differences in behavior for total current compared to LE are prominent from the results. First, the MJ current is nearly constant after ∼5 ms (Figure 3A), while LE decreases by ∼25% within 200 ms of bias pulse initiation at room temperature (Figure 3B). The decrease is more pronounced for both current and LE in the presence of acetonitrile vapor (Figure 3D) but recovers if the MJ is at rest for several minutes after a bias pulse (Figure 3C). Second, strong LE requires a bias above the HOMO−LUMO gap of $Ru(bpy)_3$, with a ∼2.7 eV threshold observed for different thicknesses and a range of electric fields (Figure 6C). The constant peak emission wavelength for the weak light emission below V = 2.7 V is distinct from and much stronger than internal photoemission,[37,38] which has a bias-dependent peak emission wavelength shown in Figure S2. Third, the rise time for LE is slower than that for the MJ current (Figure 4B) and increases significantly for thicker molecular layers (Figure 4B), with the ratio of LE/current reaching its maximum value in <1 ms for d = 12.8 nm and >20 ms for d = 28 nm (Figure 4C). Fourth, while the apparent activation energies for the MJ current and LE are similar and comparable to previous observations when d < 25 nm, the ratio of LE/current decreases by a factor of 15 between 80 and 360 K (Figure 5D). Fifth, the MJ current response is linear in plots of ln J versus $E^{1/2}$ for 1000 V/s scans and d > 10 nm (Figure 6B), while ln(LE) versus $E^{1/2}$ is nonlinear (Figure 6C). Although the current and LE approximately track each other with a bias for d < 13 nm (Figure 4D), they differ significantly when d = 20 or 28 nm. Sixth, ln J at a particular E is approximately independent of d for E > 1 MV/cm and d = 5.6 to 28 nm (Figure 6B), while LE at a given E is strongly dependent on thickness (Figure 6C). As evident in Figure 6D, LE becomes much more efficient for large d and small E, with a significant difference in behavior when d exceeds ∼15 nm. Not only do these differences indicate that two transport mechanisms operate in $Ru(bpy)_3$ MJs with d < 30 nm, but also the results are distinct from the thicker (d = 70−180 nm) light-emitting electrochemical cells studied previously[21,22,25,26] and also conventional organic semiconductors with d > 50 nm.[36] Ion motion is a requirement in the solid-state examples cited in Table 1 and is responsible for the slow rise time of light emission. Solvation of PF_6^- by acetonitrile should enhance ion mobility,[34,39,40] but decreases current and light emission in the current MJs (Figure 3D) on a 10−1000 ms time scale. In contrast to establishing a double layer to permit electrochemical charge injection, mobile PF_6^- ions in the current MJs likely screen the electrodes and partially reduce the electric field in the molecular layer interior,[34] resulting in both lower current and weaker LE. Furthermore, PF_6^- anions should be much more mobile than Ru-centered cations, thus resulting in

DOI: 10.1021/acs.jpcc.9b10076
J. Phys. Chem. C 2019, 123, 29162−29172

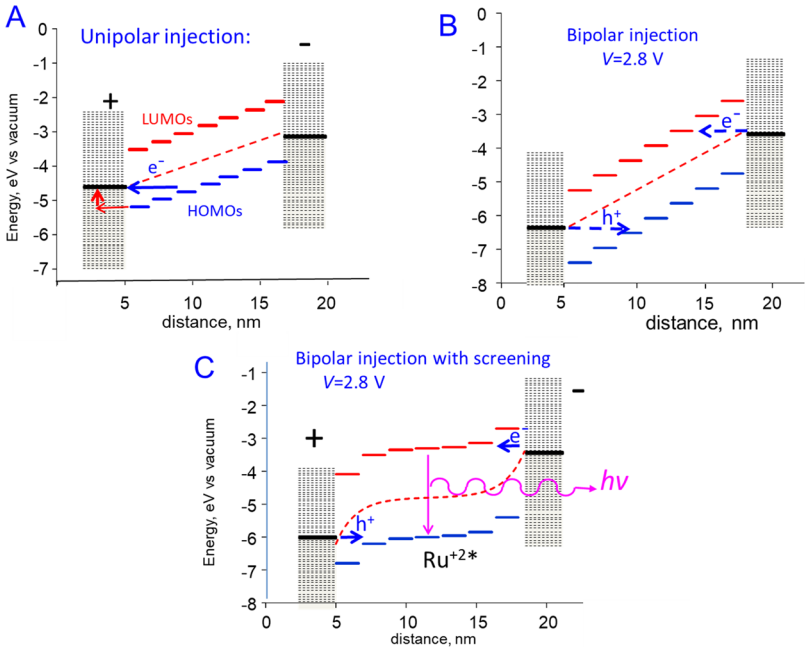

Figure 7. Energy level schematics of injection mechanisms. (A) Unipolar injection with electron transfer from HOMO to the left electrode, with the horizontal blue arrow indicating tunneling and red arrows representing activated electron transfer. (B) Bipolar injection involving both HOMO and LUMO orbitals. (C) Bipolar mechanism assisted by electrode screening, followed by migration of Ru^{+3} and Ru^{+1} to junction interior to form excited Ru^{+2}, which emits light.

an asymmetric electric field profile detrimental to bipolar injection. The ion motion occurs in a few seconds in the case of Figure 3C, consistent with the rise times listed in Table 1 for $Ru(bpy)_3$ polymers with $d > 50$ nm. Furthermore, the effects of ion motion are reversible, with the original response restored after the ions redistribute evenly at zero bias.

The linearity of ln J with $E^{1/2}$ shown in Figure 6B is not expected for electrochemical charge injection or from classical Marcus electron-transfer kinetics but is similar to that for Schottky emission across an interfacial barrier such as a metal electrode on a semiconductor. Such behavior was reported for injection from Au into Fe-terpyridine oligomers with d = 15−30 nm[13] and for carbon-based MJs when d exceeded ∼5 nm.[12,16,35] The $E^{1/2}$ dependence is likely derived from barrier lowering in an electric field, with classical Schottky emission or Poole−Frankel transport assuming thermal excitation of carriers over a field-dependent barrier.[41] The weak temperature dependence observed for carbon-based MJs implies a very low barrier for Schottky emission,[12,35] although it could be related to tunneling through a barrier at the interfaces or in the bulk film. The fact that the current density is weakly dependent on thickness for $d > 5$ nm (Figure 6B) at a given electric field, which we also observed for oligomeric molecules other than $Ru(bpy)_3$,[16] is consistent with injection-limited current. As a result, very similar current densities are observed for both 12.8 and 28 nm $Ru(bpy)_3$ MJs when they have the same field imposed. Since the positive photocurrent at zero bias (Figure 1E) implies that the HOMO energy is closer to the Fermi level,[17] electron transport involving the $Ru(bpy)_3$ HOMOs is energetically more favorable than the LUMOs. The schematic energy level diagram in Figure 7A depicts electron transfer from a $Ru(bpy_)_3$ HOMO to the positive electrode, often referred to as "hole injection".

Injection may occur via tunneling (horizontal blue arrow) or thermally activated hole generation followed by electron transfer (red arrows) and is presumably followed by rapid electron transfers from adjacent HOMOs driven by the electric field. Unipolar injection should occur when either the HOMO or LUMO is sufficiently close in energy to the electrode Fermi level and does not require the similar hole or electron barriers present in the case of $Ru(bpy)_3$. Whether the specific mechanism for hole injection is Schottky (i.e., thermionic) emission or a different process, ln J is linear with $E^{1/2}$ due to field-induced barrier lowering, and we refer to the process by the general term "unipolar injection". Unlike coherent tunneling, unipolar injection requires carriers to reside in molecular orbitals of the molecular layer, and several steps may be required to traverse molecular layers in the 5−30 nm thickness range. In addition, the exponential decrease in current for d = 5−10 nm[16] is likely an indication of an "injection-limited" current, while the overlap of ln J versus $E^{1/2}$ curves for d = 12−20 nm (Figure 6B) may represent a transition to "bulk-limited" current.

As stated in our initial report,[30] LE in $Ru(bpy)_3$ MJs is direct evidence that injection can be bipolar, with Ru^{+3} centers generated at the positive electrode and Ru^{+1} at the negative one, followed by diffusion and recombination to form excited Ru^{+2}*, which emits light. The slower rise time of LE compared to the MJ current evident in Figure 4 is likely caused by the time required for Ru^{+1} and Ru^{+3} centers to reach the junction interior and form Ru^{+2}*, which occurs by a series of electron transfers between $Ru(bpy)_3$ orbitals. As shown in Figure 7B, the HOMO and LUMO levels for $Ru(bpy)_3$ are predicted to be offset from the electrode Fermi levels by ∼1.3 eV,[30] although the photocurrent spectrum implies that the HOMO is closer. When LE and current are measured simultaneously 25 ms after initiation of a bias pulse, the ratio of LE to MJ current is related to the external quantum efficiency for photoemission, and in all cases, the efficiency varies greatly with thickness and bias (Figure 6D). The low efficiency for 8

DOI: 10.1021/acs.jpcc.9b10076
J. Phys. Chem. C 2019, 123, 29162−29172

and 13 nm devices indicates that the bipolar current is a small contribution to the total MJ current but becomes very significant for 20 and 28 nm devices. The very different field dependence of LE compared to the MJ current (Figure 6B,C) is consistent with different mechanisms once the bias exceeds the 2.67 eV HOMO−LUMO gap of $Ru(bpy)_3$ (Figure 2B,D).[30] Since the unipolar mechanism is field-dependent, its magnitude for a given bias decreases with increasing thickness. In contrast, the bipolar LE mechanism depends on the applied bias rather than the electric field and represents an increasingly larger component of the total current as d increases. The result is higher efficiency of LE for thick MJs and low bias (Figure 6D). Qualitative conclusions based on bias and thickness dependencies include the fact that the unipolar mechanism occurs in all cases studied, is field-controlled, and is the dominant component for d < 15 nm. The similarity of the electron and hole injection barriers for $Ru(bpy)_3$ enables the bipolar component, which becomes more efficient for thick films, possibly due to increased probability of radiative recombination in the molecular layer. While LE is an indicator of bipolar injection for thicker MJs, the distinct temperature dependencies for 13 and 28 nm (Figure 4D) and the change in efficiency above d = 13 nm (Figure 5D) may also result from a transition from injection-limited current for small d to bulk-limited current for d > 13 nm.

However, the mechanism depicted in Figure 7B should be field-dependent with the onset bias increasing with $Ru(bpy)_3$ thickness, contrary to the observation of a nearly constant onset bias for d = 5 to 28 nm (Figure 6C). A possible explanation for this apparent discrepancy invokes electrode screening by mobile charges, as shown in Figure 7C. Screening decreases the injection barriers and shortens the tunneling distance between the electrodes and HOMO or LUMO orbitals, thus increasing the injection rates at both electrodes. Once the threshold bias of ∼2.7 V is applied, bipolar injection can occur and is no longer field-dependent. Therefore, screening can account for the transition from field-dependent unipolar injection to bias-dependent bipolar injection and light emission. The mobile charges, which screen the electrodes, could be PF_6^- moving toward the positive electrode and away from the negative electrode, or mobile Ru^{+1} or Ru^{+3} centers formed by injection. The more rapid rise of the current and LE in the presence of acetonitrile (Figure 3C) may result from reorientation of ACN dipoles with resulting partial electrode screening or enhanced transport of PF_6^- ions. The slow, reversible decrease in LE with time in the presence of ACN may result from additional screening by PF_6^-, which causes the electric field in the molecular layer interior to decrease significantly and retard Ru^{+1} and Ru^{+3} transport. While the current results do not permit identification of the mobile charges responsible for screening, the existence of two mechanisms with distinct field and bias dependence is strong evidence that significant screening occurs.

The bipolar mechanism with screening of Figure 7C has some similarities to the electrochemical mechanism underlying photoemission in $Ru(bpy)_3$ polymers but also important differences. Most LEC and OLED devices involve electrodes with different work functions, while the current MJs have symmetric carbon electrodes. Electron injection into a LUMO or ejection from a HOMO followed by reorganization yields the same Ru^{+1} and Ru^{+3} centers as electrochemical charge transfer but becomes more efficient at lower temperatures (Figure 5C), and LE is visible even for T < 10 K. The nonlinear Arrhenius plots for both thin and thick $Ru(bpy)_3$ MJs yield apparent E_{act} values ranging from 4−90 meV, which are much lower than those reported for redox exchange in Ru polymers (200−500 meV)[42] and transport in OLEDs (∼500 meV),[43] indicating that transport in $Ru(bpy)_3$ thin films differs mechanistically from that when d > 50 nm. The near-zero apparent E_{act} below 200 K for $Ru(bpy)_3$ and other aromatic molecules with d > 5 nm[16,35] indicates that activationless injection by tunneling or field emission can dominate the observed current, in contrast to the widely accepted activated electron transfer typical of electrochemical charge injection. As temperature increases above ∼200 K, an activated process contributes to the injection rate, possibly including classical Schottky emission. We are currently investigating the relative contribution of thermal and activationless injection mechanisms, as well the specific physical principles, which determine the effect of structure and orbital energies on the injection rate and the directly related device current.

In addition to being significantly different from solid-state light-emitting electrochemical devices, the current bipolar mechanism is quite distinct from that in OLEDs. Nearly all existing OLEDs consist of different metal contacts with different work functions to inject holes at one electrode and electrons at the other.[6,7,44,45] They also have "hole transport" and "electron transport" layers between the electrodes and the light-emitting molecular layer, which strive to make the two carriers equal in number to maximize efficiency. In contrast, the current $Ru(bpy)_3$ light-emitting MJs have a single molecular component, symmetric electrodes (both disordered carbon), and nearly symmetric carbon/molecule interfaces. As a consequence, emission is very similar in spectrum and magnitude for either bias polarity on the same device,[30] with no requirement for additional layers. Compared to electrochemical (LEC) and OLED devices, the $Ru(bpy)_3$ molecular junctions are simpler and much thinner, with symmetric electrodes and a single active molecular layer. They exhibit fast response and high efficiency and operate with minimal additional bias voltage over that required to overcome the HOMO−LUMO gap and result in bipolar injection.

■ ASSOCIATED CONTENT

Supporting Information

The Supporting Information is available free of charge at https://pubs.acs.org/doi/10.1021/acs.jpcc.9b10076.

Emission spectra and LE transients at additional temperatures, fast current transients, and silicon detector response (PDF)

■ AUTHOR INFORMATION

Corresponding Author

*E-mail: mccreery@ualberta.ca. Tel.: 780-492-9594.

ORCID

Colin Van Dyck: 0000-0003-2853-3821
Shailendra K. Saxena: 0000-0001-7156-3407
Jean-Christophe Lacroix: 0000-0002-7024-4452
Richard L. McCreery: 0000-0002-1320-4331

Notes

The authors declare no competing financial interest.

DOI: 10.1021/acs.jpcc.9b10076
J. Phys. Chem. C 2019, 123, 29162−29172

■ ACKNOWLEDGMENTS

This work was supported by the University of Alberta, the National Research Council of Canada, and the Natural Sciences and Engineering Research Council and Alberta Innovates. ANR (France) is gratefully acknowledged for its financial support of this work (ANR-15-CE09-0001-01). Frederic Lafolet provided the $Ru(bpy)_3$ amino precursor essential for device fabrication.

■ REFERENCES

(1) Katsouras, I.; Najafi, A.; Asadi, K.; Kronemeijer, A. J.; Oostra, A. J.; Koster, L. J. A.; de Leeuw, D. M.; Blom, P. W. M. Charge Transport in Poly(P-Phenylene Vinylene) at Low Temperature and High Electric Field. *Org. Electron.* **2013**, *14*, 1591−1596.

(2) Ringk, A.; Li, X.; Gholamrezaie, F.; Smits, E. C. P.; Neuhold, A.; Moser, A.; van der Marel, C.; Gelinck, G. H.; Resel, R.; de Leeuw, D. M.; Strohriegl, P. N-Type Self-Assembled Monolayer Field-Effect Transistors and Complementary Inverters. *Adv. Funct. Mater.* **2013**, *23*, 2016−2023.

(3) Defaux, M.; Gholamrezaie, F.; Wang, J.; Kreyes, A.; Ziener, U.; Anokhin, D. V.; Ivanov, D. A.; Moser, A.; Neuhold, A.; Salzmann, I.; Resel, R.; de Leeuw, D. M.; Meskers, S. C. J.; Moeller, M.; Mourran, A. Solution-Processable Septithiophene Monolayer Transistor. *Adv. Mater.* **2012**, *24*, 973−978.

(4) Mandal, S.; Noh, Y.-Y. Printed Organic Thin-Film Transistor-Based Integrated Circuits. *Semicond. Sci. Technol.* **2015**, *30*, 064003.

(5) Liao, C.; Yan, F. Organic Semiconductors in Organic Thin-Film Transistor-Based Chemical and Biological Sensors. *Polym. Rev.* **2013**, *53*, 352−406.

(6) Yang, X.; Zhou, G.; Wong, W.-Y. Functionalization of Phosphorescent Emitters and Their Host Materials by Main-Group Elements for Phosphorescent Organic Light-Emitting Devices. *Chem. Soc. Rev.* **2015**, *44*, 8484−8575.

(7) Fan, C.; Yang, C. Yellow/Orange Emissive Heavy-Metal Complexes as Phosphors in Monochromatic and White Organic Light-Emitting Devices. *Chem. Soc. Rev.* **2014**, *43*, 6439−6469.

(8) Braga, D.; Erickson, N. C.; Renn, M. J.; Holmes, R. J.; Frisbie, C. D. High-Transconductance Organic Thin-Film Electrochemical Transistors for Driving Low-Voltage Red-Green-Blue Active Matrix Organic Light-Emitting Devices. *Adv. Funct. Mater.* **2012**, *22*, 1623−1631.

(9) Sedghi, G.; Esdaile, L. J.; Anderson, H. L.; Martin, S.; Bethell, D.; Higgins, S. J.; Nichols, R. J. Comparison of the Conductance of Three Types of Porphyrin−Based Molecular Wires: *β*,meso,*β*−Fused Tapes, meso−Butadiyne−Linked and Twisted meso−meso Linked Oligomers. *Adv. Mater.* **2012**, *24*, 653−657.

(10) Sedghi, G.; García-Suárez, V. M.; Esdaile, L. J.; Anderson, H. L.; Lambert, C. J.; Martín, S.; Bethell, D.; Higgins, S. J.; Elliott, M.; Bennett, N.; Macdonald, J. E.; Nichols, R. J. Long-Range Electron Tunnelling in Oligo-Porphyrin Molecular Wires. *Nat. Nanotechnol.* **2011**, *6*, 517−523.

(11) Nguyen, Q. V.; Martin, P.; Frath, D.; Della Rocca, M. L.; Lafolet, F.; Bellinck, S.; Lafarge, P.; Lacroix, J.-C. Highly Efficient Long-Range Electron Transport in a Viologen-Based Molecular Junction. *J. Am. Chem. Soc.* **2018**, *140*, 10131−10134.

(12) Yan, H.; Bergren, A. J.; McCreery, R.; Della Rocca, M. L.; Martin, P.; Lafarge, P.; Lacroix, J. C. Activationless Charge Transport across 4.5 to 22 Nm in Molecular Electronic Junctions. *Proc. Natl. Acad. Sci. U. S. A.* **2013**, *110*, 5326−5330.

(13) Karipidou, Z.; Branchi, B.; Sarpasan, M.; Knorr, N.; Rodin, V.; Friederich, P.; Neumann, T.; Meded, V.; Rosselli, S.; Nelles, G.; Wenzel, W.; Rampi, M. A.; von Wrochem, F. Ultrarobust Thin-Film Devices from Self-Assembled Metal−Terpyridine Oligomers. *Adv. Mater.* **2016**, *28*, 3473−3480.

(14) Taherinia, D.; Smith, C. E.; Ghosh, S.; Odoh, S. O.; Balhorn, L.; Gagliardi, L.; Cramer, C. J.; Frisbie, C. D. Charge Transport in 4 nm Molecular Wires with Interrupted Conjugation: Combined Experimental and Computational Evidence for Thermally Assisted Polaron Tunneling. *ACS Nano* **2016**, *10*, 4372−4383.

(15) Smith, C. E.; Odoh, S. O.; Ghosh, S.; Gagliardi, L.; Cramer, C. J.; Frisbie, C. D. Length-Dependent Nanotransport and Charge Hopping Bottlenecks in Long Thiophene-Containing Π-Conjugated Molecular Wires. *J. Am. Chem. Soc.* **2015**, *137*, 15732−15741.

(16) Tefashe, U. M.; Nguyen, Q. V.; Morteza Najarian, A.; Lafolet, F.; Lacroix, J.-C.; McCreery, R. L. Orbital Control of Long-Range Transport in Conjugated and Metal-Centered Molecular Electronic Junctions. *J. Phys. Chem. C* **2018**, *122*, 29028−29038.

(17) Morteza Najarian, A.; Bayat, A.; McCreery, R. L. Orbital Control of Photocurrents in Large Area All-Carbon Molecular Junctions. *J. Am. Chem. Soc.* **2018**, *140*, 1900−1909.

(18) Tuccitto, N.; Ferri, V.; Cavazzini, M.; Quici, S.; Zhavnerko, G.; Licciardello, A.; Rampi, M. A. Highly Conductive 40-Nm-Long Molecular Wires Assembled by Stepwise Incorporation of Metal Centres. *Nat. Mater.* **2009**, *8*, 41−46.

(19) Van Nguyen, Q.; Lafolet, F.; Martin, P.; Lacroix, J. C. Ultrathin Molecular Layer Junctions Based on Cyclometalated Ruthenium Complexes. *J. Phys. Chem. C* **2018**, *122*, 29069−29074.

(20) Sedghi, G.; Sawada, K.; Esdaile, L. J.; Hoffmann, M.; Anderson, H. L.; Bethell, D.; Haiss, W.; Higgins, S. J.; Nichols, R. J. Single Molecule Conductance of Porphyrin Wires with Ultralow Attenuation. *J. Am. Chem. Soc.* **2008**, *130*, 8582−8583.

(21) Kalyuzhny, G.; Buda, M.; McNeill, J.; Barbara, P.; Bard, A. J. Stability of Thin-Film Solid-State Electroluminescent Devices Based on Tris(2,2′-Bipyridine)Ruthenium(Ii) Complexes. *J. Am. Chem. Soc.* **2003**, *125*, 6272−6283.

(22) Buda, M.; Kalyuzhny, G.; Bard, A. J. Thin-Film Solid-State Electroluminescent Devices Based on Tris(2,2′-Bipyridine)-Ruthenium(Ii) Complexes. *J. Am. Chem. Soc.* **2002**, *124*, 6090−6098.

(23) Liu, C.-Y.; Bard, A. J. Individually Addressable Submicron Scale Light-Emitting Devices Based on Electroluminescence of Solid Ru(Bpy)3(Clo4)2 Films. *J. Am. Chem. Soc.* **2002**, *124*, 4190−4191.

(24) Maness, K. M.; Masui, H.; Wightman, R. M.; Murray, R. W. Solid State Electrochemically Generated Luminescence Based on Serial Frozen Concentration Gradients of RuIII/II and RuII/I Couples in a Molten Ruthenium 2,2′-Bipyridine Complex. *J. Am. Chem. Soc.* **1997**, *119*, 3987−3993.

(25) Handy, E. S.; Pal, A. J.; Rubner, M. F. Solid-State Light-Emitting Devices Based on the Tris-Chelated Ruthenium(II) Complex. 2. Tris(Bipyridyl)Ruthenium(II) as a High-Brightness Emitter. *J. Am. Chem. Soc.* **1999**, *121*, 3525−3528.

(26) Gao, F. G.; Bard, A. J. Solid-State Organic Light-Emitting Diodes Based on Tris(2,2′-Bipyridine)Ruthenium(II) Complexes. *J. Am. Chem. Soc.* **2000**, *122*, 7426−7427.

(27) Zhao, W.; Liu, C.-Y.; Wang, Q.; White, J. M.; Bard, A. J. Effect of Residual Solvent on Ru(Bpy)3(Clo4)2-Based Light-Emitting Electrochemical Cells. *Chem. Mater.* **2005**, *17*, 6403−6406.

(28) Rudmann, H.; Rubner, M. F. Single Layer Light-Emitting Devices with High Efficiency and Long Lifetime Based on Tris(2,2′ Bipyridyl) Ruthenium(II) Hexafluorophosphate. *J. Appl. Phys.* **2001**, *90*, 4338−4345.

(29) Lee, J. K.; Yoo, D. S.; Handy, E. S.; Rubner, M. F. Thin Film Light Emitting Devices from an Electroluminescent Ruthenium Complex. *Appl. Phys. Lett.* **1996**, *69*, 1686−1688.

(30) Tefashe, U. M.; Nguyen, Q. V.; Lafolet, F.; Lacroix, J.-C.; McCreery, R. L. Robust Bipolar Light Emission and Charge Transport in Symmetric Molecular Junctions. *J. Am. Chem. Soc.* **2017**, *139*, 7436−7439.

(31) Morteza Najarian, A.; Szeto, B.; Tefashe, U. M.; McCreery, R. L. Robust All-Carbon Molecular Junctions on Flexible or Semi-Transparent Substrates Using "Process-Friendly" Fabrication. *ACS Nano* **2016**, *10*, 8918−8928.

(32) Ivashenko, O.; Bergren, A. J.; McCreery, R. L. Light Emission as a Probe of Energy Losses in Molecular Junctions. *J. Am. Chem. Soc.* **2016**, *138*, 722−725.

(33) Ivashenko, O.; Bergren, A. J.; McCreery, R. L. Monitoring of Energy Conservation and Losses in Molecular Junctions through

DOI: 10.1021/acs.jpcc.9b10076
J. Phys. Chem. C 2019, 123, 29162−29172

Characterization of Light Emission. *Adv. Electron. Mater.* **2016**, *2*, 1600351.
(34) Chandra Mondal, P.; Tefashe, U. M.; McCreery, R. L. Internal Electric Field Modulation in Molecular Electronic Devices by Atmosphere and Mobile Ions. *J. Am. Chem. Soc.* **2018**, *140*, 7239−7247.
(35) Morteza Najarian, A.; McCreery, R. L. Structure Controlled Long-Range Sequential Tunneling in Carbon-Based Molecular Junctions. *ACS Nano* **2017**, *11*, 3542−3552.
(36) Shen, Y.; Hosseini, A. R.; Wong, M. H.; Malliaras, G. G. How to Make Ohmic Contacts to Organic Semiconductors. *ChemPhysChem* **2004**, *5*, 16−25.
(37) Fereiro, J. A.; Kondratenko, M.; Bergren, A. J.; McCreery, R. L. Internal Photoemission in Molecular Junctions: Parameters for Interfacial Barrier Determinations. *J. Am. Chem. Soc.* **2015**, *137*, 1296−1304.
(38) Fereiro, J. A.; McCreery, R. L.; Bergren, A. J. Direct Optical Determination of Interfacial Transport Barriers in Molecular Tunnel Junctions. *J. Am. Chem. Soc.* **2013**, *135*, 9584−9587.
(39) Das, B. C.; Szeto, B.; James, D. D.; Wu, Y.; McCreery, R. L. Ion Transport and Switching Speed in Redox-Gated 3-Terminal Organic Memory Devices. *J. Electrochem. Soc.* **2014**, *161*, H831−H838.
(40) Das, B. C.; Pillai, R. G.; Wu, Y.; McCreery, R. L. Redox-Gated Three-Terminal Organic Memory Devices: Effect of Composition and Environment on Performance. *ACS Appl. Mater. Interfaces* **2013**, *5*, 11052−11058.
(41) Sze, S. M.; Ng, K. K. *Physics of Semiconductor Devices*. 2nd ed.; Wiley: New York, 1981.
(42) Ranganathan, S.; Murray, R. W. Comparison of Thermal and Optical Electron-Transfer Barriers in Ruthenium Redox Polyether Melts. *J. Phys. Chem. B* **2004**, *108*, 19982−19989.
(43) Züfle, S.; Altazin, S.; Hofmann, A.; Jäger, L.; Neukom, M. T.; Brütting, W.; Ruhstaller, B. Determination of Charge Transport Activation Energy and Injection Barrier in Organic Semiconductor Devices. *J. Appl. Phys.* **2017**, *122*, 115502.
(44) Kordt, P.; van der Holst, J. J. M.; Al Helwi, M.; Kowalsky, W.; May, F.; Badinski, A.; Lennartz, C.; Andrienko, D. Modeling of Organic Light Emitting Diodes: From Molecular to Device Properties. *Adv. Funct. Mater.* **2015**, *25*, 1955−1971.
(45) Kulkarni, A. P.; Tonzola, C. J.; Babel, A.; Jenekhe, S. A. Electron Transport Materials for Organic Light-Emitting Diodes. *Chem. Mater.* **2004**, *16*, 4556−4573.

DOI: 10.1021/acs.jpcc.9b10076
J. Phys. Chem. C 2019, 123, 29162−29172